Int. J. Therm. Sci. (2000) 39, 886–895

S1290-0729(00)01174-1/FLA

The effects of thermal non-equilibrium and inlet temperature on two-phase flow pressure drop type instabilities in an upflow boiling system

L. Cao [a], S. Kakaç [a], H.T. Liu [a]*, P.K. Sarma [b]

[a] *Department of Mechanical Engineering, University of Miami, Coral Gables, FL 33124, USA*

[b] *College of Engineering, Gandhi Institute of Technology and Management, Visakhapatnam 530 045, India*

(Received 12 May 2000, accepted 5 July 2000)

Abstract — In this paper a theoretical model for the two-phase flow pressure drop type instabilities in an upflow boiling system is presented. The thermal non-equilibrium effect between the two phases is included assuming the enthalpy profile in the subcooled boiling region. The system of differential equations describing the single-phase and boiling regions of the system (drift-flux model) is solved using finite difference method for the steady state characteristics of the system over a wide range of operating conditions. Upon obtaining the steady state characteristics, the dynamic formulation of the pressure drop type oscillation is solved numerically. The modeling results are verified by the experimental findings. The effect of the thermal non-equilibrium on the steady state characteristics, stability boundaries and oscillation periods at different heat inputs and inlet temperatures are presented as being compared with the experimental measurements as well as the results obtained from the thermal equilibrium model. © 2000 Éditions scientifiques et médicales Elsevier SAS

two-phase flow / pressure drop type instabilities / thermal non-equilibrium effect / subcooled boiling

Nomenclature

A_c	cross-sectional area	m^2
C_0	distribution parameter	
c_p	specific heat	$J{\cdot}kg^{-1}{\cdot}K^{-1}$
D_h	diameter of the heater	m
f_f	single phase liquid friction factor	
f_m	two-phase mixture friction factor	
F_m	two-phase flow friction multiplier	
G	mass flux	$kg{\cdot}m^{-2}{\cdot}s^{-1}$
g	acceleration due to gravity	$m{\cdot}s^{-2}$
h	enthalpy	$J{\cdot}kg^{-1}$
h_{fs}	saturated liquid enthalpy	$J{\cdot}kg^{-1}$
Δh_{sub}	inlet subcooling	$J{\cdot}kg^{-1}$
Δh_{fg}	latent heat of vaporization	$J{\cdot}kg^{-1}$
J	volumetric flux	$m{\cdot}s^{-1}$
K_{in}	inlet orifice coefficient (from main tank to surge tank)	
L_{out}	length of system from surge tank outlet to the exit of exit restriction	m
L_{in}	length of system from main tank outlet to surge tank inlet	m
Δl	axial length along heated section from z_0 to z_1	m
$\dot{m}$	mass flow rate	$kg{\cdot}s^{-1}$
P	pressure	bar
ΔP	pressure drop	bar
P_e	exit pressure	bar
P_t	surge tank pressure	bar
Pe	Peclet number	
P_{ta0}	steady state pressure of the air in the surge tank	bar
q	heat flux	$W{\cdot}m^{-2}$
Q	heat input	W
t	time	s
T	temperature	K
T_{in}	liquid bulk temperature at the inlet of the heater tube	°C
T_L	liquid bulk temperature	K
T_0	liquid bulk temperature at the z_0	K
ΔT_s	temperature difference $(T_{sat} - T_0)$	K

* Correspondence and reprints.
hliu@coeds.eng.miami.edu

$\Delta T_{s,in}$	inlet subcooling ($T_{sat} - T_{in}$)	K
u	velocity	$m \cdot s^{-1}$
$u_{f,in}$	liquid inlet velocity	$m \cdot s^{-1}$
V_{at0}	volume of air in surge tank at steady state	m^3
V_{gj}	drift velocity of vapor	$m \cdot s^{-1}$
x	vapor quality	
x_{eq}	vapor quality assuming thermodynamic equilibrium	
z_1	axial coordinate at point of $T_L = T_{sat}$.	m
z	axial coordinate at point along heated section measured from the inlet	m
z_0	axial coordinate at point of net vapor generation	m

Greek symbols

α	void fraction	
Γ_g	mass rate of vapor generation per unit volume	$kg \cdot m^{-3} \cdot s^{-1}$
μ	dynamic viscosity of the fluid	Pa·s
ρ	density	$kg \cdot m^{-3}$
ξ_h	heated perimeter	m
σ	surface tension	$N \cdot m^{-1}$

Subscripts

e	exit
eq	equilibrium assumption
f	liquid phase
g	vapor phase
i	node index in discretization scheme
in	inlet
j	interface index in discretization scheme
lo	liquid alone with the mass flow rate of the total two-phase flow
m	two-phase mixture
mt	main tank
out	outlet
sat	saturation
tp	two-phase
w	wall

1. INTRODUCTION

Two-phase flow systems are common in energy and chemical industries. It is well known that two-phase instabilities can introduce operational and control problems to steam generators, boiling water reactors and various chemical process equipments. Therefore, it is essential to be able to predict the onset and characteristics of the oscillations in terms of operating conditions. There have been many analytical and experimental investigations on the two-phase flow instabilities as can be found in the review papers by Bouré et al. [1], Bergles [2], Lahey and Drew [3], Yadigaroglu [4] and Kakaç and Liu [5]. Stenning [6] and Stenning and Veziroglu [7] investigated and identified three types of dynamic instabilities, namely, density wave type, pressure drop type, and thermal oscillations in a single channel upflow boiling system.

Pressure drop type oscillations occur in a system with a sufficient compressible volume upstream of the boiling channel, when the system pressure drop decreases with an increase in the mass flow rate. Compressible volume exists in long test sections ($L/d > 150$ [8]) or can be artificially introduced by placing a surge tank upstream of the test section [7]. Being caused by the dynamic interaction between the compressible volume and the channel, the period and amplitude of the pressure drop type oscillations are much larger than those of the density wave oscillations [7, 8].

Although this particular type of instability has been studied extensively in the past [9–14], the effect of the thermal non-equilibrium between the phases, i.e. the local bulk temperature differences between the two phases has been neglected. However, in practice subcooled boiling region in a heated channel exists. Without taking subcooled boiling region into consideration, the transition from the liquid region to the boiling region is artificially delayed, which will introduce errors in predicting the stability boundary and oscillatory characteristics of the pressure drop type oscillations. Convective subcooled boiling has been studied extensively by researchers over the world [15–21], and several correlations were presented corresponding to different range of operating conditions and working fluid.

The objective of this work is to study theoretically the effect of the thermal non-equilibrium on the steady-state and oscillatory characteristics of the pressure drop type instabilities of boiling flow in a single vertical channel.

2. THERMAL NON-EQUILIBRIUM EFFECTS

Figure 1 diagrammatically shows the variations of the liquid bulk temperature as well as the mass quality along the axial length of a uniformly heated channel.

The liquid bulk temperature starts to increase linearly at the inlet of heated channel because of the uniform heat flux distribution. In thermal equilibrium model (as shown with the dotted lines in *figure 1*), the bulk liquid temperature increases linearly up to the saturation value

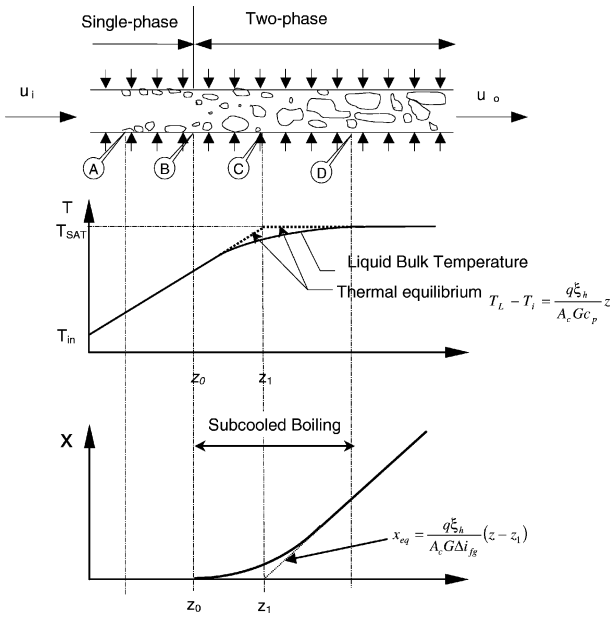

Figure 1. Schematic representation of subcooled boiling in convective boiling.

(point C) and all the heat added to the system would go to raise the temperature of the liquid only. After the saturation point, the liquid bulk temperature remains constant at the saturation temperature and all the heat added goes to generate vapor.

A real system, however, will not be in thermodynamic equilibrium. The vapor bubble generation starts while the liquid bulk temperature is very much below the saturation temperature with high local subcooling (point A — onset of the nucleation), since the wall temperature there is above saturation and there exists a thin layer of superheated liquid film in the near vicinity of the heating surface. The bubbles nucleate, grow, and eventually collapse after they penetrate into the subcooled liquid core, thus, the vapor void fraction cannot increase significantly until the point (point B — net vapor generation point) where the liquid subcooling is low and the bubbles can move to the core of the flow. As shown in *figure 1*, the liquid bulk temperature beyond this point is lower than that predicted by the thermal equilibrium model because part of the heat added to the system is used to generate vapor. Therefore, the quality and the bulk liquid temperature will cease to be linear with distance in the subcooled boiling region. Since the rate of temperature rise is decreased, the bulk liquid temperature will reach saturation temperature further downstream from point z_1 at point D. Beyond point D, the quality will increase again linearly with distance.

2.1. Subcooled boiling region

It is evident from the foregoing that the axial quality and temperature distributions are related and either distribution can be used to describe the state of thermal nonequilibrium. Consider a steady, one-dimensional flow of a two-phase mixture with constant properties and assume that the effects of the kinetic and potential energies can be neglected, the problem of determining the temperature distribution in the liquid can be formulated [15, 18] by considering:

- Conservation of mass for the mixture

$$G = G_{\mathrm{f}} + G_{\mathrm{g}} \tag{1}$$

- Continuity equation for the vapor

$$\frac{\partial G_{\mathrm{g}}}{\partial z} = \Gamma_{\mathrm{g}} \tag{2}$$

- Energy equation for the mixture

$$G_{\mathrm{f}} \frac{\partial h_{\mathrm{f}}}{\partial z} + G_{\mathrm{g}} \frac{\partial h_{\mathrm{g}}}{\partial z} + \Gamma_{\mathrm{g}} \Delta h_{\mathrm{fg}} = \frac{q \xi_{\mathrm{h}}}{A_{\mathrm{c}}} \tag{3}$$

- Equation of state for the vapor

$$h_{\mathrm{g}} = h_{\mathrm{g}}(P, T) \tag{4}$$

- Constitutive equation of evaporation in the bubbly regime

$$\Gamma_{\mathrm{g}} = \frac{\xi_{\mathrm{h}}}{A_{\mathrm{c}}} \int_{z_0}^{z_1} \frac{\mathrm{d}m(z, z')}{\mathrm{d}z} J(z') \, \mathrm{d}z' \tag{5}$$

In equation (5), the vapor generation rate depends on the rate of nucleation $J(z')$ and on the bubble growth $m(z, z')$, where $J(z')$ is the rate of bubble formation per unit area at a location z' in the duct, and $m(z, z')$ gives the mass at z of a bubble that nucleated at z'.

Due to the uncertainties in determining the heterogeneous bubble nucleation rate and the subsequent bubble growth law, the use of the above formal approach proposed by Zuber et al. [15, 17, 18] is not warranted to obtain the temperature distribution. Therefore, the constitutive equation for the rate of vapor generation is required. Instead of the formal approach, an alternative approach is to make realistic assumption about the liquid bulk enthalpy, h_{f}, and then determine the rate of vapor generation from the mixture energy equation (equation (3)).

Zuber et al. [15, 17, 18] suggested the following liquid enthalpy distribution that satisfies the boundary

conditions at $z = z_0$ and $z \to \infty$:

$$\frac{h_f(z) - h_f(z_0)}{h_f(z_1) - h_f(z_0)} = 1 - \exp\left(-\frac{z - z_0}{\Delta l}\right) \quad (6)$$

where the characteristic length Δl is given by

$$\Delta l = z_1 - z_0 = \frac{GA_c[h_{fs} - h(z_0)]}{q\xi_h} \quad (7)$$

Based on equation (6), the equations for predicting the quality and average void fraction (average over the cross-sectional area of the duct) in subcooled boiling region of the two-phase mixture were given by [15, 17, 18]

$$\langle\alpha\rangle = x\left\{C_0\frac{\rho_f - \rho_g}{\rho_f}x + \left[C_0 + \frac{V_{gj}}{u_{f,in}}\right]\frac{\rho_g}{\rho_f}\right\}^{-1} \quad (8)$$

$$x = \frac{q\xi_h\Delta l}{GA_c\Delta h_{fg}} \cdot \frac{z^+ - T^+}{1 + c_p\Delta T_s(1 - T^+)/\Delta h_{fg}} \quad (9)$$

where

$$T^+ = \frac{T_l(z) - T(z_0)}{T_{sat}(z_0) - T(z_0)} \quad (10)$$

$$z^+ = \frac{z - z_0}{\Delta l} \quad (11)$$

which took into consideration the local relative velocity (V_{gj}), the concentration and flow profile (C_0) and the temperature profile (T^+).

2.2. Net vapor generation point

According to the non-equilibrium model, the boiling boundary is the point where significant vapor generation starts and its distance from the inlet can be given by [19]

- for $\Delta h_{sub} \geq \Delta h(z_0)$

$$z_0 = \frac{GA_c[\Delta h_{sub} - \Delta h(z_0)]}{q\xi_h} \quad (12)$$

where

$$\Delta h(z_0) = 0.0022\frac{qD_h c_{p,f}}{K_f} \quad \text{if } Pe \leq 70\,000 \quad (13)$$

and

$$\Delta h(z_0) = 154\frac{q}{\rho_f u_{f,in}} \quad \text{if } Pe \geq 70\,000 \quad (14)$$

- for $\Delta h_{sub} \leq \Delta h(z_0)$

$$z_0 = 0 \quad (15)$$

3. STEADY STATE CHARACTERISTICS

Mathematical representation of the experimental system is shown in *figure 2*, where five distinct regions are identified along the system.

The components upstream of the inlet of the heated channel are lumped together and considered as the first region. The whole length of the heater is divided into the subcooled liquid region and the boiling two-phase fluid region, which are numbered regions 2 and 3. Region 4 extends from the exit of the heater to the exit restriction. The exit restriction is treated as region 5.

3.1. Governing equations

Drift-flux model is used to formulate the problem in the two-phase mixture region. The time-smoothed, one-dimensional conservation equations as derived by Ishii and Zuber [22] are:

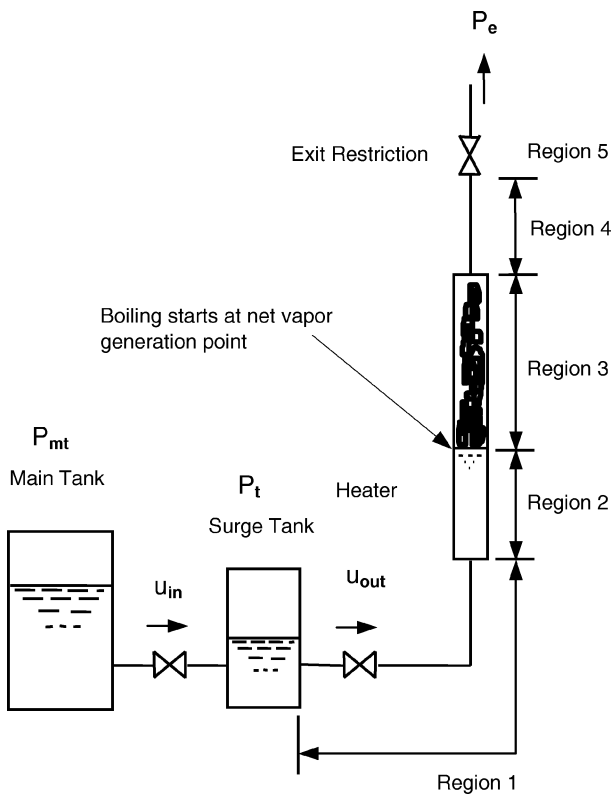

Figure 2. Mathematical representation of the physical system.

- Conservation of mass of the mixture

$$\frac{\partial(\rho_{\mathrm{m}} u_{\mathrm{m}})}{\partial z} = 0 \tag{16}$$

- Conservation of mass of the vapor phase

$$\frac{\partial(\alpha \rho_{\mathrm{g}} u_{\mathrm{g}})}{\partial z} = \Gamma_{\mathrm{g}} \tag{17}$$

- Conservation of momentum of the mixture (neglecting the effect of surface tension)

$$\rho_{\mathrm{m}} u_{\mathrm{m}} \frac{\partial u_{\mathrm{m}}}{\partial z} = -\frac{\partial P}{\partial z} - \frac{f_{\mathrm{m}}}{2D_{\mathrm{h}}} \rho_{\mathrm{m}} u_{\mathrm{m}}^2 + g\rho_{\mathrm{m}} - \frac{\partial}{\partial z}\left(\frac{\rho_{\mathrm{f}} - \rho_{\mathrm{m}}}{\rho_{\mathrm{m}} - \rho_{\mathrm{g}}} \frac{\rho_{\mathrm{f}}\rho_{\mathrm{g}}}{\rho_{\mathrm{m}}} V_{\mathrm{g}j}^2\right) \tag{18}$$

- Conservation of energy of the mixture (neglecting the effect of the kinetic and potential energy)

$$\rho_{\mathrm{m}} u_{\mathrm{m}} \frac{\partial h_{\mathrm{m}}}{\partial z} = \frac{q_{\mathrm{w}} \xi_{\mathrm{h}}}{A_{\mathrm{c}}} - \frac{\partial}{\partial z}\left(\frac{\rho_{\mathrm{f}} - \rho_{\mathrm{m}}}{\rho_{\mathrm{m}}} \frac{\rho_{\mathrm{f}}\rho_{\mathrm{g}}}{\rho_{\mathrm{f}} - \rho_{\mathrm{g}}} V_{\mathrm{g}j}(h_{\mathrm{g}} - h_{\mathrm{f}})\right) \tag{19}$$

The mixture density ρ_{m}, the mixture velocity u_{m}, and the mixture enthalpy h_{m} are defined as

$$\rho_{\mathrm{m}} = \alpha\rho_{\mathrm{g}} + (1-\alpha)\rho_{\mathrm{f}} \tag{20}$$

$$u_{\mathrm{m}} = \frac{\alpha\rho_{\mathrm{g}} u_{\mathrm{g}}}{\rho_{\mathrm{m}}} + \frac{(1-\alpha)\rho_{\mathrm{f}} u_{\mathrm{f}}}{\rho_{\mathrm{m}}} \tag{21}$$

$$h_{\mathrm{m}} = \frac{\alpha\rho_{\mathrm{g}} h_{\mathrm{g}}}{\rho_{\mathrm{m}}} + \frac{(1-\alpha)\rho_{\mathrm{f}} h_{\mathrm{f}}}{\rho_{\mathrm{m}}} \tag{22}$$

In single-phase liquid region, the liquid is considered to be incompressible and one-dimensional flow with constant thermodynamic and transport properties. Therefore, the conservation equations are reduced to:

- Continuity equation

$$\frac{\partial u_{\mathrm{f}}}{\partial z} = 0 \tag{23}$$

- Momentum equation

$$\rho_{\mathrm{f}} u_{\mathrm{f}} \frac{\partial u_{\mathrm{f}}}{\partial z} = -\frac{\partial P}{\partial Z} - \frac{f_{\mathrm{f}}}{2D_{\mathrm{h}}} \rho_{\mathrm{f}} u_{\mathrm{f}}^2 + g\rho_{\mathrm{f}} \tag{24}$$

- Energy equation

$$u_{\mathrm{f}} \frac{\partial h_{\mathrm{f}}}{\partial z} = \frac{q_{\mathrm{w}} \xi_{\mathrm{h}}}{\rho_{\mathrm{f}} A_{\mathrm{c}}} \tag{25}$$

3.2. The kinematic correlation for void fraction

The model used in the present study was proposed by Zuber and Findlay [23]. According to their analysis, the vapor velocity u_{g} is related to the volumetric flux as

$$u_{\mathrm{g}} = C_0 J + V_{\mathrm{g}j} \tag{26}$$

where $C_0 = \langle\alpha\rangle\langle J\rangle / \langle\alpha J\rangle$ is the distribution parameter, $V_{\mathrm{g}j}$ is the drift velocity of the vapor phase with respect to the center of mass of the mixture and J is the volumetric flux defined as

$$J = u_{\mathrm{f}}(1-\alpha) + u_{\mathrm{g}}\alpha \tag{27}$$

The following expressions are reported to give good results irrespective of the flow pattern [23]:

$$C_0 = 1.13 \tag{28}$$

$$V_{\mathrm{g}j} = 1.41\left[\frac{\sigma g(\rho_{\mathrm{f}} - \rho_{\mathrm{g}})}{\rho_{\mathrm{f}}^2}\right]^{1/4} \tag{29}$$

3.3. Exit restriction

The exit restriction is a sharp-edged orifice located at the outlet of the heater, with diameter 2.64 mm.

The following correlation was developed (equation (30)) by modifying the separated flow model of two-phase fluid flowing through the orifice [14]:

$$\frac{\Delta P_{\mathrm{tp}}}{\Delta P_{\mathrm{lo}}} = 1 + \left(\frac{v_{\mathrm{g}}}{v_{\mathrm{f}}} - 1\right) c_1 x^{c_2} \tag{30}$$

The constants c_1 and c_2 are obtained by correlating the experimental results. It is found that c_1 increases with the heat input, while c_2 keeps constant (see *table I*).

TABLE I
c_1 and c_2 for different heat inputs.

Heat input (W)	c_1	c_2
1 000	2.4	1.5
800	2.3	1.5
600	1.5	1.5
400	1.0	1.5

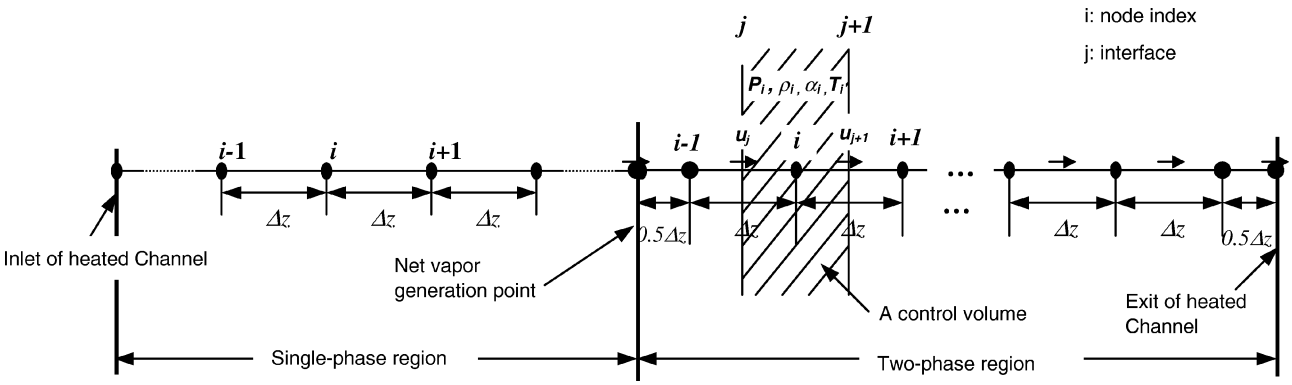

Figure 3. Discretization diagram of the heated channel.

3.4. Finite difference solution of the steady state characteristics

The mass and momentum equations are discretized in the space coordinate and the numerical calculation is carried out from the surge tank to the system exit by matching process in the space coordinate. *Figure 3* shows the discretization diagram of the single-phase and two-phase regions of the heated channel. In the two-phase boiling region, staggered grids are used — velocity is defined at the control volume interface, while other parameters and properties are defined at the center of the control volume (node).

Equations (31) and (32) are the discretization forms of the mass and momentum equations:

$$\frac{\rho_{\mathrm{m},j+1}u_{\mathrm{m},j+1}-\rho_{\mathrm{m},j}u_{\mathrm{m},j}}{\Delta z}=0 \tag{31}$$

$$(\rho_{\mathrm{m},j+1}u_{\mathrm{m},j+1})\frac{u_{\mathrm{m},j+1}-u_{\mathrm{m},j}}{\Delta z} = -\frac{P_i-P_{i-1}}{\Delta z}-\frac{f_{\mathrm{m}}G}{2\rho_{\mathrm{m},i}D_{\mathrm{h}}}-g\rho_{\mathrm{m},i}-\frac{S_{j+1}-S_j}{\Delta z} \tag{32}$$

where

$$S=\frac{\rho_{\mathrm{f}}-\rho_{\mathrm{m}}}{\rho_{\mathrm{m}}-\rho_{\mathrm{g}}}\frac{\rho_{\mathrm{f}}\rho_{\mathrm{g}}}{\rho_{\mathrm{m}}}V_{\mathrm{g}j}^2$$

and

$$S_{j+1}=\frac{S_{i+1}+S_i}{2},\qquad \rho_{j+1}=\frac{\rho_{i+1}+\rho_i}{2} \tag{33}$$

$$S_j=\frac{S_i+S_{i-1}}{2},\qquad \rho_j=\frac{\rho_i+\rho_{i-1}}{2} \tag{34}$$

The trial and error method is used by assuming different value of P_{t} to arrive at the given value of P_{e} within given errors. *Figure 4* shows the flowchart of the program implemented for solving the steady state characteristics of the system.

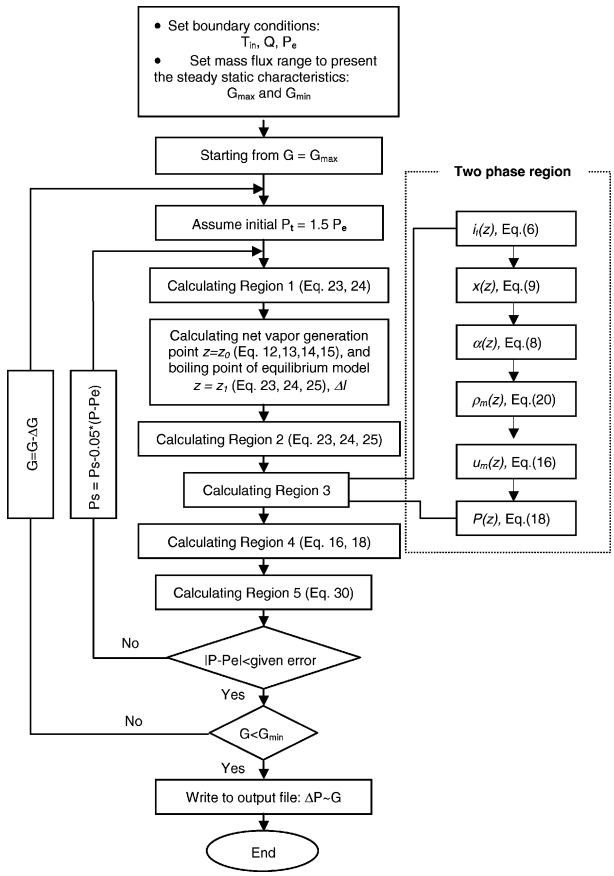

Figure 4. Program flow chart for calculating steady state characteristics of the system.

To include the subcooled boiling effect, the net vapor generation point is calculated and taken as the starting

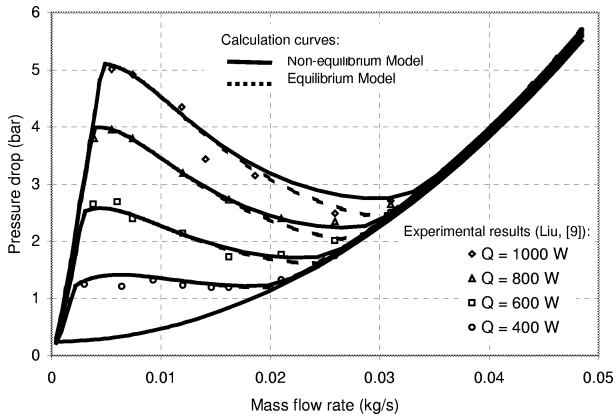

Figure 5. Steady state characteristics with different heat inputs ($T_{in} = 23\,^{\circ}\mathrm{C}$).

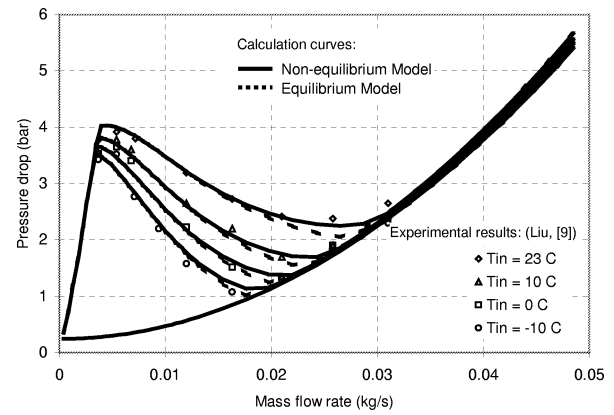

Figure 6. Steady state characteristics with different inlet temperatures ($Q = 800$ W).

point of boiling, instead of the point where the bulk liquid temperature reaches the saturation temperature corresponding to the local pressure. The whole length of the heater is then divided by the net vapor generation point into the single-phase section and the two-phase boiling section. Each section is computed using their finite difference forms of governing equations. Appropriate state and constitutive equations are chosen according to the state of the fluid.

The steady state characteristics curves of the system are shown in *figures 5* and *6*, as comparisons of the non-equilibrium model with the experiments (Liu [9]) and equilibrium model. In *figure 5*, different curves correspond to the different heat inputs, while in *figure 6* the curves correspond to the different inlet temperatures of the fluid. It is seen in these figures that the model calculation fits the experimental results quite well and is capable of predicting the steady state behavior of the system under different operating conditions. Comparing the calculation curves of non-equilibrium and equilibrium models, it is shown in these figures that non-equilibrium model better matches the experimental data, and the improvement is more distinctive when the heat input and inlet temperature are higher.

4. DYNAMIC SIMULATIONS OF THE PRESSURE DROP TYPE INSTABILITY

4.1. Dynamic model of the pressure drop type oscillation

Pressure drop type oscillations have relatively low frequency, and their periods are usually much longer than the residence time of the fluid particles in the system. Consequently, quasi-static condition is assumed in modeling the pressure drop type instabilities in the boiling system, which means the transient operating points can be obtained as a series of steady state points. In addition, the following assumptions about the physical system are made to form the present dynamic model:

- the temperature inside the surge tank is constant during oscillations,
- the heat input to the fluid is constant during the oscillations, i.e. the dynamics of the heater wall is neglected.

For surge tank, the continuity equation can be written as [10, 11]

$$\frac{\mathrm{d}P_t}{\mathrm{d}t} = \frac{(P_t - P_{tv})^2 A_c}{P_{ta0} V_{a0}} (u_{in} - u_{out}) \tag{35}$$

The momentum equation between the main tank and the surge tank is written as

$$\frac{\mathrm{d}u_{in}}{\mathrm{d}t} = \frac{1}{\rho_f L_{in}} \left[(P_{mt} - P_t) - K_{in} \rho_f u_i^2 \right] \tag{36}$$

where K_{in} is the inlet restriction coefficient of the valve between the main and surge tanks.

With the quasi-static assumption of the pressure drop type oscillation, the momentum equation between the surge tank and the system exit can be written as

$$\frac{\mathrm{d}u_{out}}{\mathrm{d}t} = \frac{1}{\rho_f L_{out}} \left[(P_t - P_e) - (P_t - P_e)_s \right] \tag{37}$$

where $(P_t - P_e)_s$ is the steady state pressure drop given in the earlier section.

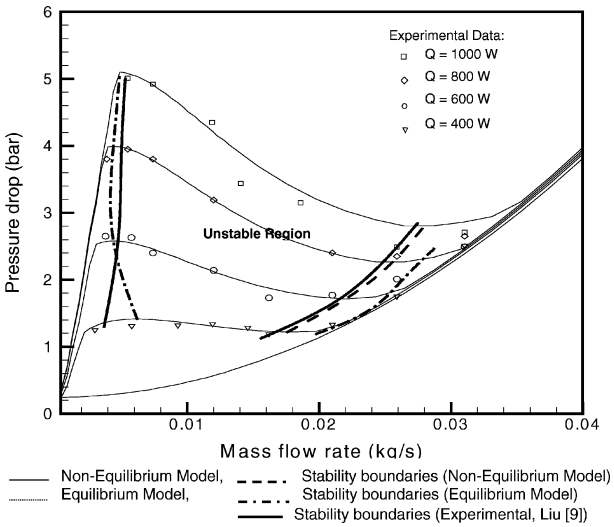

Figure 7. Stability boundaries (different heat inputs at $T_{in} = 23\,^{\circ}C$).

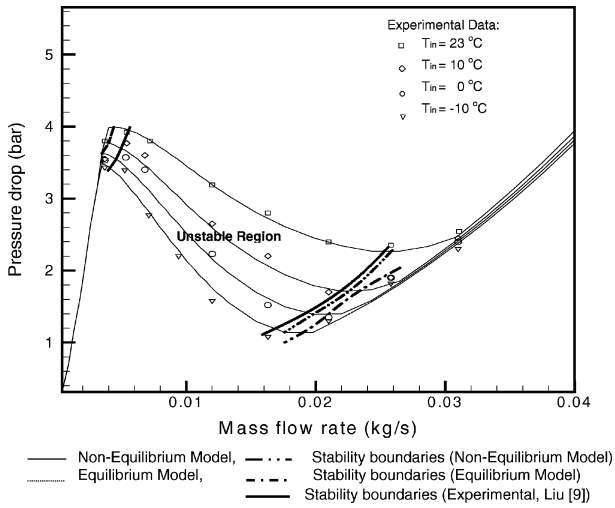

Figure 8. Stability boundaries (different inlet temperatures at $Q = 800$ W).

Equations (35)–(37) form the dynamic model of the system under the pressure drop type oscillation. This ordinary differential equation set is numerically solved using the mathematical solver (ODE) in MATLAB.

4.2. Solutions to the model

4.2.1. Stability boundaries of the system

Small pressure perturbation to the surge tank pressure is imposed to the system under steady-state of the different operating conditions, and the time variations of pressure and mass flow rate of the perturbed system are traced to determine the point where oscillations start under certain operating conditions. Stable system returns back to the steady state under perturbation, while the unstable system presents limit cycles of the pressure and mass flow rate variation. The system stability boundaries are marked in the steady state pressure drop versus mass flow rate plane, as shown in *figures 7* and *8*.

The experimental data [9] of the onset of flow oscillation corresponding to various heat inputs imposed on the system (*figure 7*) and inlet temperatures (*figure 8*) are compared with the results of the non-equilibrium model, as well as the equilibrium model. As can be seen clearly in the figures, the non-equilibrium model approaches closer the experimental results (Liu [9]) than the equilibrium model, and the equilibrium theory predicts a more unstable system than the non-equilibrium model does. Both the non-equilibrium and equilibrium model give more conservative solutions comparing with the experimental results, i.e. the models present more broad range of mass flow rates under which the oscillations occur.

TABLE II
Comparison of experimental and theoretical results of pressure drop oscillations. Bare tube; tube I.D. = 7.5 mm; exit restriction: 1.6 mm; inlet temperature: 23 °C.

Heat input (W)	Mass flow rate ($g \cdot s^{-1}$)	Theoretical (non-equilibrium) period (s)	Theoretical (equilibrium) period (s)	Experimental (Liu [9]) period (s)
400	11.89	14.2	15.1	13.5
600	11.89	17.2	21.0	17.0
800	11.89	31.5	36.8	28.5
1 000	11.89	38.0	51.5	32.5

4.2.2. Nonlinear simulations of the pressure drop oscillations

The numerical solutions to the dynamic model (equations (35)–(37)) for the oscillation period of the surge tank pressure under different inlet temperatures are listed in *tables II–V*. The results predicted by the non-equilibrium and equilibrium models as well as the experimental measurements (Liu [9]) are compared in *table II* under the same mass flow rate ($\dot{m} = 11.89\ g \cdot s^{-1}$) but different heat inputs ($Q = 400, 600, 800, 1\,000$ W).

It is seen from *table II* that, at $T_{in} = 23\,^{\circ}C$, the higher the heat input, the larger the period of the oscillation. Both the non-equilibrium model and the equilibrium model predict larger periods as being compared with the experimental data, but the non-equilibrium model fits the

TABLE III
Comparison of theoretical results of pressure drop oscillations. Bare tube; tube I.D. = 7.5 mm; exit restriction: 1.6 mm; inlet temperature: 10 °C.

Heat input (W)	Mass flow rate ($g \cdot s^{-1}$)	Theoretical (non-equilibrium) period (s)	Theoretical (equilibrium) period (s)
400	11.89	34.8	37.6
600	11.89	38.2	44.7
800	11.89	37.3	45.2
1 000	11.89	35.8	44.6

TABLE IV
Comparison of theoretical results of pressure drop oscillations. Bare tube; tube I.D. = 7.5 mm; exit restriction: 1.6 mm; inlet temperature: 0 °C.

Heat input (W)	Mass flow rate ($g \cdot s^{-1}$)	Theoretical (non-equilibrium) period (s)	Theoretical (equilibrium) period (s)
400	11.89	57.5	65.0
600	11.89	50.4	56.0
800	11.89	48.4	54.8
1 000	11.89	43.1	52.4

TABLE V
Comparison of theoretical results of pressure drop oscillations. Bare tube; tube I.D. = 7.5 mm; exit restriction: 1.6 mm; inlet temperature: −10 °C.

Heat input (W)	Mass flow rate ($g \cdot s^{-1}$)	Theoretical (non-equilibrium) period (s)	Theoretical (equilibrium) period (s)
400	11.89	stable	stable
600	11.89	67.5	71.0
800	11.89	58.4	66.9
1 000	11.89	51.8	60.7

experimental data quite well, especially at lower heat input ($Q = 400$ and 600 W).

Under different inlet temperatures, the comparisons of the non-equilibrium model to the equilibrium model in predicting the oscillation periods are listed in *tables III–V* ($T_{in} = 10\,°C$, 0 °C and −10 °C, respectively). At $T_{in} = 10\,°C$ (*table III*), the heat input to the system has little effect on the oscillation period, and equilibrium model presents larger periods than the non-equilibrium model does under different heat inputs. When the inlet temperature is further decreased below 10 °C, as is shown in *tables IV* and *V*, the oscillation period decreases as the heat input increases, which is opposite to the case in *table II*. However, the equilibrium model always gives larger period comparing to the non-equilibrium model under same inlet temperature and heat input.

5. CONCLUDING REMARKS

The drift flux model is adopted to predict the steady state characteristics of the boiling system, and the finite difference solution of this model for the steady-state characteristics agrees satisfactorily with the experimental measurements (Liu [9]).

The results of the non-equilibrium and equilibrium models are compared with the experimental steady-state curves of the system, and it is found that the non-equilibrium theory approaches closer to the experimental data. In subcooled boiling region, the higher the heat input and the fluid inlet temperature, the larger the difference between the calculations from the non-equilibrium and equilibrium models.

The dynamic model of the pressure-drop type oscillations can reasonably predict the stability boundaries and periods of the oscillations. It is concluded that the non-equilibrium theory predicts the experimental data quite satisfactorily, and it is a better model compared with the equilibrium model.

REFERENCES

[1] Bouré J.A., Bergles A.E., Tong L.S., Review of two-phase instabilities, Nuclear Engineering and Design 25 (1973) 165–184.

[2] Bergles A.E., Review of instabilities in two-phase systems, in: Kakaç, Mayinger, Veziroglu (Eds.), Two-phase Flow and Heat Transfer, Hemisphere, Washington, DC, 1977.

[3] Lahey Jr. R.T., Drew D.A., An assessment of the literature related to LWR instability modes, NUREG/CR-1414, 1980.

[4] Yadigaroglu G., Two-phase flow instabilities and propagation phenomena, in: Dehaye, Giot, Riethmuller (Eds.), Thermohydraulics of Two-phase Flow Systems for Industrial Design and Nuclear Engineering, Hemisphere, 1981.

[5] Kakaç S., Liu H.T., Two-phase flow dynamic instabilities in boiling systems, in: Chen X.J., Veziroglu T.N., Tien C.L. (Eds.), Multi-phase Flow and Heat Transfer, Vol. 1, 1991, pp. 403–444.

[6] Stenning A.H., Instabilities in the flow of a boiling liquid, Journal of Basic Engineering, Trans. ASME 86(D) (1964) 213–221.

[7] Stenning A.H., Veziroglu T.N., Flow oscillation modes in forced convection boiling, in: Proc. Heat Transfer and Fluid Mechanics Institute, Stanford University Press, 1965, p. 301.

[8] Maulbetsch J.S., Griffith P., System-induced instabilities in forced convection flow with subcooled boiling, in: 3rd International Heat Transfer Conference, Chicago, IL, Vol. 4, 1966, p. 247.

[9] Liu H.T., Parametric study of two-phase flow instabilities in a force-convective boiling upflow system, M.S. Thesis, University of Miami, Coral Gables, FL, 1989.

[10] Veziroglu T.N., Kakaç S., Two-phase flow instabilities, Final Report, NSF Project CME 79-20018, Clean Energy Research Institute, University of Miami, 1983.

[11] Dogan T., Kakaç S., Veziroglu T.N., Analysis of forced boiling flow instabilities in a single-channel upflow system, Int. J. Heat Fluid Flow 4 (1983) 145–156.

[12] Padki M.M., Liu H.T., Kakaç S., Two-phase flow pressure-drop type and thermal oscillations, Int. J. Heat Fluid Flow 12 (1991) 240–248.

[13] Liu H.T., Pressure drop type and thermal oscillations in convective boiling systems, Ph.D. Thesis, University of Miami, Coral Gables, FL, 1993.

[14] Cao L., Kakaç S., Liu H.T., Sarma P.K., Theoretical analysis of pressure-drop type instabilities in an upflow boiling system with an exit restriction, submitted to J. Heat Mass Tran. (2000).

[15] Zuber N., Staub F.W., Bijwaard G., Vapor void fraction in subcooled boiling and saturated boiling systems, in: Proc. 3rd International Heat Transfer Conference, Vol. 5, AIChE, New York, 1966, p. 24.

[16] Bijwaard G., Staub F.W., Zuber N., A program of two-phase flow investigation, Eleventh Quarterly Report, October–December, General Electric Co., San Jose, CA, Report No. GEAP 5067, Euratom Report No. EURAEC 1575, 1965.

[17] Zuber N., Dougherty D.E., Liquid metals challenge to the traditional methods of two-phase flow investigations, in: Symposium on Two-phase Flow Dynamics, Eindhoven, Vol. 1, EURATOM, Brussels, 1967, p. 1091.

[18] Kroeger P.G., Zuber N., An analysis of the effects of various parameters on the average void fractions in subcooled boiling, Int. J. Heat Mass Tran. 11 (1968) 211–232.

[19] Saha P., Zuber N., Point of net vapor generation and vapor void fraction in subcooled boiling, in: Heat Transfer 1974, Proc. 5th International Heat Transfer Conference, Vol. 4, 1974, pp. 175–179.

[20] Campolunghi F., Cumo M., Palazzi G., Urbani C., Subcooled and bulk boiling correlations for thermal design of steam generators, CNEN RT/ING 77:10, Comitato Nazionale Per L'Energía Nucleare, Milan, Italy, 1977.

[21] Rouhani S.Z., Calculation of steam volume fraction in subcooled boiling, in: Natl. Heat Transfer Conf., Vol. 3, 1967, ASME paper 67-HT-31.

[22] Ishii M., Zuber N., Thermally induced flow instabilities in two-phase mixtures, in: Proc. 4th International Heat Transfer Conference, Paris, Elsevier, Amsterdam, 1970, Paper B5.11.

[23] Zuber N., Findlay J., Average volumetric concentration in two-phase flow system, J. Heat Tran. 87C (1965) 453.